Electrically reconfigurable metamaterial absorber operating in C band

Le Van Long[1, 3], Bui Son Tung[1, 2*], Bui Xuan Khuyen[1, 2**],
Bui Huu Nguyen[4], Vu Dinh Lam[1**]

[1]Graduate University of Science and Technology, Vietnam Academy of Science and Technology, 18 Hoang Quoc Viet, Cau Giay, Hanoi 100000, Vietnam;
[2]Institute of Materials Science, Vietnam Academy of Science and Technology, 18 Hoang Quoc Viet, Cau Giay, Hanoi 100000, Vietnam;
[3]Joint Russia-Vietnam Tropical Science and Technology, Hanoi 122103, Vietnam;
[4]Department of Physics, Hanoi University of Mining and Geology, 18 Pho Vien, Duc Thang ward, Bac Tu Liem District, Hanoi, Vietnam.
*Corresponding authors: tungbs@ims.vast.ac.vn
**Co-Corresponding authors: khuyenbx@ims.vast.ac.vn; lamvd@gust-edu.vast.vn
Received 22 Jun. 2023; Revised 13 Sep. 2023; Accepted 10 Nov. 2023; Published 25 Nov. 2023.
DOI: https://doi.org/10.54939/1859-1043.j.mst.91.2023.63-72

ABSTRACT

Reconfigurable metamaterial absorbers have garnered significant attention due to their ability to actively manipulate absorption characteristics without modifying the underlying geometrical structure. This study proposes a straightforward approach for the creation of electrically reconfigurable metamaterial absorbers through the integration of varactor diodes. The presented work encompasses two distinct types of absorbers: single-band and dual-band metamaterial absorbers. By leveraging an external voltage, effective control over absorption frequencies in the C-band is achieved. The underlying principle is elucidated, wherein controlled variations of effective parameters within the integrated diode facilitate the adjustment of the magnetic resonance frequency of the metamaterial absorber. Consequently, our research might contribute to the advancement of efficient, dynamic, and adaptive metamaterial-based devices endowed with enhanced functionalities for diverse applications in the realms of telecommunications, electromagnetic shielding, and beyond.

Keywords: Electrically reconfigurable metamaterial absorber; Varactor diode; Magnetic resonance.

1. INTRODUCTION

Metamaterials are artificial materials engineered to have electromagnetic properties not found in naturally occurring materials. They are composed of sub-wavelength structures that interact with electromagnetic waves in unique ways, enabling unprecedented control over the propagation and manipulation of electromagnetic radiation. Metamaterials have found applications in a wide range of fields, including antenna design [1, 2], imaging [3, 4], cloaking [5, 6], and sensing [7, 8]. In addition to these fields, since its initial development by Landy et al. [9], metamaterial absorbers (MAs) have emerged as a highly intriguing topic due to their outstanding advantages, including high absorption [10, 11], frequency flexibility [12-14], and compact size [15, 16].

One of the key challenges in developing metamaterials is their fixed electromagnetic properties, which limit their versatility in different applications. Therefore, the development of reconfigurable metamaterials, which can be dynamically tuned or switched between different electromagnetic properties, has emerged as an important area of research [17, 18]. Reconfigurable metamaterials offer the ability to adapt to changing environments or operational requirements, enabling a wide range of applications that require tunability or switchability. They have been demonstrated in various forms,

including mechanically tunable structures [19], electrically tunable structures [20], and optically tunable structures [21]. The importance of reconfigurable metamaterials lies in their potential to unlock new applications that require the ability to dynamically manipulate electromagnetic waves.

Electrically reconfigurable metamaterials offer distinct advantages when compared to other forms of reconfigurable metamaterials, including mechanical, thermal, magnetic, and optical counterparts. Firstly, these metamaterials offer fast and dynamic reconfiguration capabilities, enabling real-time adjustments and adaptability [22]. By leveraging electrical signals, such metamaterials can achieve rapid response times and on-the-fly changes in their properties. Secondly, electrical control provides precise modulation, allowing for fine-tuned adjustments of voltage levels, currents, or electric fields. This level of precision is challenging to attain using alternative reconfiguration mechanisms. Additionally, electrically reconfigurable metamaterials exhibit excellent scalability and ease of integration into existing electronic systems, as electrical control mechanisms are compatible with a diverse range of electronic devices [23, 24]. This compatibility facilitates seamless integration, enabling the development of large-scale arrays or networks of reconfigurable metamaterials.

In our work, we present the design of both single- and dual-band absorbers, showcasing their ability to effectively tune absorption frequencies within the C band by simply adjusting the applied voltage. Furthermore, we conduct simulations to analyze and elucidate the absorption mechanism based on the induced field distribution. Our findings offer a pathway to the development of efficient and actively tunable meta-devices with potential applications in electromagnetic interference shielding, radar stealth, and telecommunications.

2. STRUCTURE DESIGN AND SIMULATION

Figure 1 illustrates the unit-cell design of MAs, which function as absorbers for both single- and dual-band applications. These MAs consist of a periodic array of unit-cells arranged in their respective sample planes. Essentially, both types of MAs comprise three layers: a continuous metallic layer at the back, a continuous dielectric layer in the middle, and a patterned metallic layer at the front, which incorporates inductors and diodes.

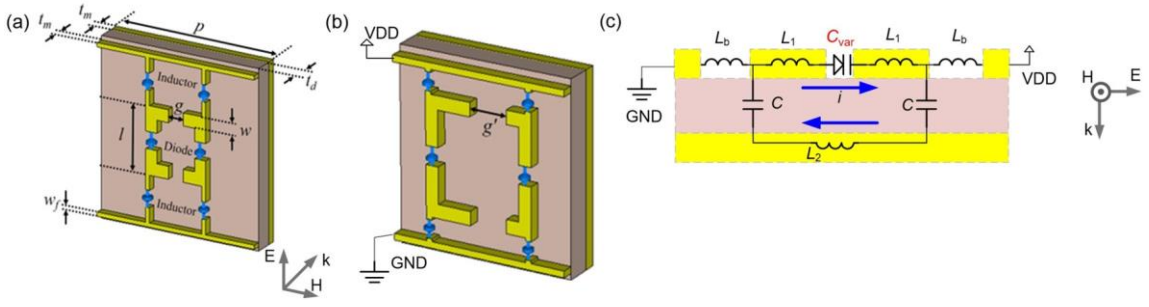

Figure 1. *Unit cells of (a) single- and (b) dual-band MAs. (c) Simplified equivalent circuit diagram of MA at resonance frequency.*

For the single-band MA, the unit-cell structure of the front layer adopts a symmetric four-gap split-ring resonator (s-SRR) with two varactor diodes integrated within two of

the gaps to control the resonance frequency of the resonators. Metallic feeding lines, designed on the top and bottom of the s-SRR, apply a direct current (DC) voltage to the varactor diodes. To prevent microwave frequency signals from interfering with the DC bias line, inductors are placed between the feeding lines and the s-SRR. The inductors exhibit high impedance at the investigated frequency region, effectively isolating the microwave frequency signal while allowing the DC bias to pass through with minimal impedance. The design of the dual-band MA follows a similar approach to that of the single-band MA. However, the top and bottom gaps of the resonator extend towards the right, creating an asymmetric four-gap split-ring resonator (a-SRR). The specific geometrical parameters of the proposed single- and dual-band MAs are provided in table 1 and table 2, respectively.

Table 1. *Geometrical parameters of proposed single-band MA.*

p (mm)	t_d (mm)	t_m (mm)	l (mm)	w (mm)	g (mm)	w_f (mm)
21	2.4	0.035	8	1.5	2	0.5

Table 2. *Geometrical parameters of proposed dual-band MA.*

p (mm)	t_d (mm)	t_m (mm)	l (mm)	w (mm)	g (mm)	g' (mm)	w_f (mm)
14.6	2.2	0.035	9	1.05	2	3.1	0.5

The simulation was conducted using the CST Microwave Studio software [25] to analyze the proposed MAs in the frequency range within the C band, specifically from 4 to 8 GHz. The middle dielectric layer was composed of FR-4 material, possessing a relative permittivity of 4.3 and a loss tangent of 0.025. Copper, known for its conductivity of 5.8×10^7 S/m, was selected as the material for both the front and back layers. The inductance of AC isolated inductor is 100 μH. To control the electromagnetic behavior of MAs, varactor diodes SMV2019-079LF are used, which can be simplified as a RLC series circuit with its equivalent circuit parameters at different bias voltages listed in table 3 [26]. Here, the magnitude of the applied voltage is increased from 0 V to 19 V, and the minus sign of the applied voltage indicates that a reverse voltage is being applied to the diode to adjust its value. The main role of integrated varactor diodes is to create a variable capacitance, which alters the resonance frequency of MA, as shown in the simplified equivalent circuit diagram of MA in Fig. 1(c).

Table 3. *Equivalent circuit parameters for the varactor diode [26].*

Voltage (V)	C (pF)	R (Ω)	L (nH)
0	2.31	4.51	0.7
−4	0.84	4.04	0.7
−7	0.55	3.66	0.7
−14	0.31	2.86	0.7
−19	0.24	2.38	0.7

During the simulation, a plane wave was stimulated to propagate perpendicular to the plane of MA. The electric field was vertically polarized and aligned parallel to the diode-integrated gaps, while the magnetic field was directed horizontally and followed the gaps without diodes. To establish a periodic array on the sample plane, the unit-cell boundary was implemented.

The absorption characteristics were determined by employing the formula $A(\omega) = 1 - R(\omega) - T(\omega)$, wherein $R(\omega) = |S_{11}(\omega)|^2$ and $T(\omega) = |S_{21}(\omega)|^2$ represented the reflection and transmission coefficients, respectively. Notably, our specific design featured a continuous copper plate as the back layer, thereby achieving complete suppression of microwave transmission. Consequently, the absorption simplifies to $A(\omega) = 1 - R(\omega)$.

3. RESULTS AND DISCUSSION

3.1. Reconfigurable single-band absorption

Figure 3 illustrates the absorption spectra of the proposed single-band MA. Initially, in the absence of any applied voltage on the varactor diode, the MA exhibits a prominent absorption peak in the C band at a frequency of 4.7 GHz, accompanied by an absorption magnitude of 91%. Upon the application of a bias voltage of -4 V, a noticeable shift in the absorption peak occurs, resulting in a higher frequency of 5.4 GHz. Simultaneously, the absorption magnitude increases significantly to reach a value of 99%. Subsequently, by gradually increasing the bias voltage, the absorption of the MA continues to exhibit a blue-shifted behavior. At bias voltages of -7 V, -14 V, and -19 V, the corresponding absorption frequencies are measured to be 5.7 GHz, 6.1 GHz, and 6.4 GHz, respectively. Notably, despite these shifting frequencies, the absorption magnitudes remain relatively high, with values of 99%, 97%, and 92% for the respective bias voltages mentioned above. This signifies that the MA maintains its absorptive capabilities effectively, even under different levels of bias voltage. These observations highlight the potential of the proposed single-band MA as a versatile and frequency-tunable absorber in the C band.

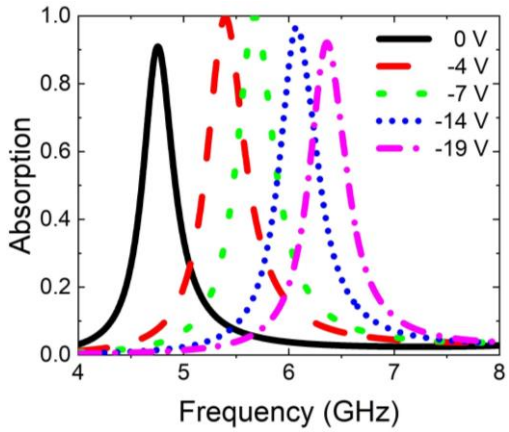

Figure 2. *Dependence of absorption spectrum of single-band MA on the applied voltage.*

To elucidate the absorption characteristics during the alteration of the applied voltage, simulations were conducted to visualize the induced currents on the MA under two distinct conditions: 0 V and -19 V, as depicted in Figs. 3 and 4, respectively. At both applied voltages, the induced currents on the front and back copper layers exhibit an anti-parallel orientation, signifying the excitation of magnetic resonance at the absorption frequency. Moreover, the currents primarily concentrate within the regions corresponding to the positions of the s-SRRs. This observation implies that the magnetic resonance is primarily induced by the s-SRR structure, while the influence of the feeding line on the resonance is relatively insignificant.

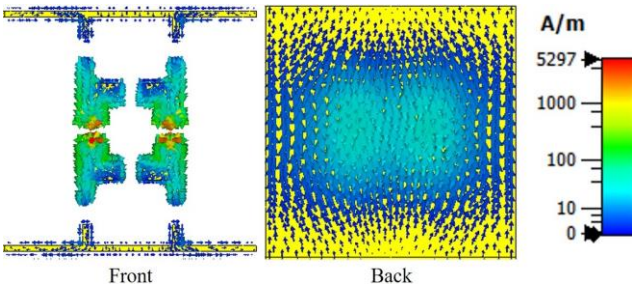

Figure 3. *Surface-current distribution on the MA at the absorption frequency of 4.7 GHz corresponding to the applied voltage of 0 V.*

Since the absorption peaks observed at both applied voltages are magnetic resonance induced by s-SRRs, the shift in absorption frequency is attributed to the modulation of the varactor diode through the applied bias voltage. Specifically, the diode capacitance decreases as the magnitude of the applied voltage increases. It is widely recognized that the magnetic resonance of MA can be represented by an equivalent LC resonance model, with the resonance frequency being inversely proportional to the effective capacitance of the structure [27, 28]. In the proposed MA structure, the diode capacitance also contributes to the effective capacitance of MA. Therefore, a reduction in the diode capacitance results in a decrease in the effective capacitance, leading to an increase in the magnetic resonance frequency. As a consequence, the absorption peak shifts towards a higher frequency when the applied voltage is increased.

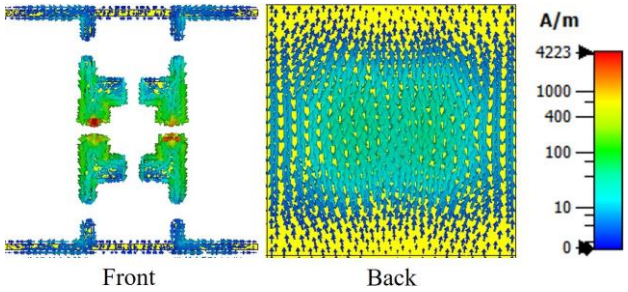

Figure 4. *Surface-current distribution on the MA at the absorption frequency of 6.4 GHz corresponding to the applied voltage of 19 V.*

3.2. Reconfigurable dual-band absorption

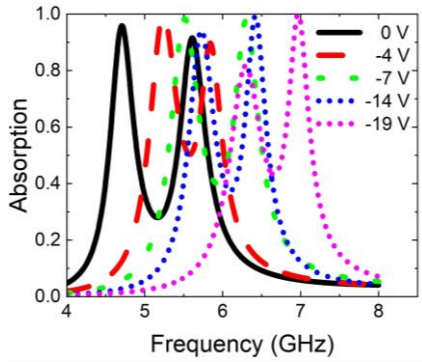

Figure 5. *Dependence of absorption spectrum of dual-band MA on the applied voltage.*

For a reconfigurable dual-band absorption, the MA structure is modified as depicted in Fig. 1(b). The influence of applied voltage on the absorption spectrum of the dual-band MA is investigated and presented in Fig. 5. By introducing asymmetry to the resonator, the a-SRR exhibits two distinct absorption peaks in the absence of applied voltage. The first peak is observed at 4.7 GHz with an absorption of 95.8%, while the second peak appears at 5.6 GHz with an absorption of 91.5%. Upon the application of a voltage of -4 V, the dual-band absorption spectrum shifts towards higher frequency regions. Consequently, the first and second absorption peaks reach 99.8% and 90% at 5.2 GHz and 5.8 GHz, respectively. The blue-shift trend persists as the applied voltage increases. Notably, the dual-band MA maintains an absorption level above 90% throughout the tuning process, even up to an applied voltage of -14 V. However, for an applied voltage of -19 V, the absorption of the first peak slightly reduces to 81.6%, while the absorption of the second peak remains high. The specific absorption magnitudes and frequencies of the dual-band MA are summarized in table 4.

Table 4. *Absorption properties of dual-band MA at various applied voltages.*

Voltage (V)	1st peak		2nd peak	
	Frequency (GHz)	Absorption	Frequency (GHz)	Absorption
0	4.7	95.8%	5.6	91.5%
-4	5.2	99.8%	5.8	90%
-7	5.5	98.3%	6.3	97.7%
-14	5.7	94%	6.4	98.8%
-19	6.3	81.6%	6.9	99.9%

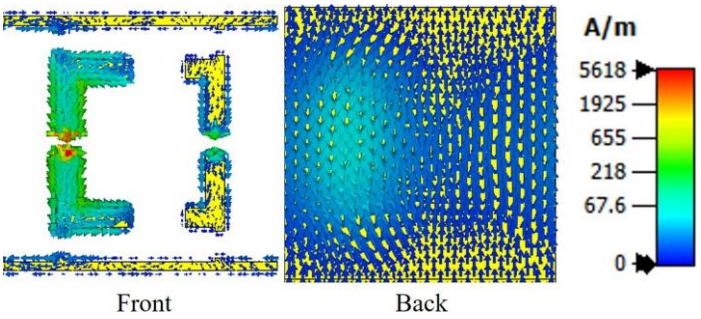

Figure 6. *Surface-current distribution on the MA at the first absorption frequency of 4.7 GHz corresponding to the applied voltage of 0 V.*

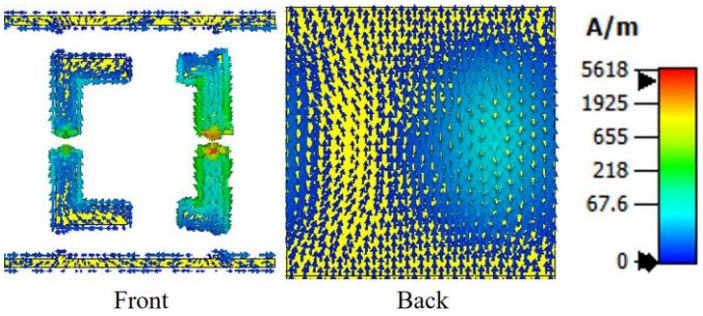

Figure 7. *Surface-current distribution on the MA at the second absorption frequency of 5.6 GHz corresponding to the applied voltage of 0 V.*

In order to provide further insights into the resonance characteristics of the dual-band MA, the induced currents are simulated and visualized, as depicted in Figs. 6 to 8. Figure 6 displays the distribution of surface currents on the copper layers at the first absorption frequency, while Fig. 7 presents the corresponding currents at the second absorption frequency, both in the absence of applied voltage. Analogous to the behavior observed in single-band MA, the induced currents on the front and back layers exhibit anti-parallel orientations at both resonance frequencies, confirming the excitation of magnetic resonances that give rise to the absorption peaks. Notably, at the first resonance frequency, the currents predominantly localize within the regions corresponding to the positions of the left sections of the a-SRR, whereas at the second resonance frequency, they concentrate primarily within the regions corresponding to the positions of the right sections of the a-SRR.

This observation is consistent with the findings at the applied voltage of -19V, where the left and right sections of the a-SRR induce the first and second resonances, respectively. Consequently, it can be deduced that by introducing asymmetry to the resonator, each section of the resonator interacts differently with the incident wave at distinct frequencies, thereby giving rise to the dual-band absorption phenomenon. These outcomes provide valuable evidence elucidating the resonance nature of the dual-band MA structure and contribute to a comprehensive understanding of its underlying physical mechanisms.

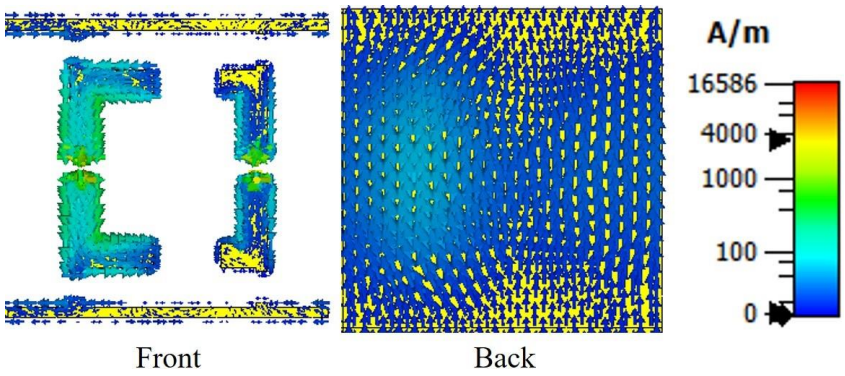

Figure 8. *Surface-current distribution on the MA at the first absorption frequency of 6.3 GHz corresponding to the applied voltage of 19V.*

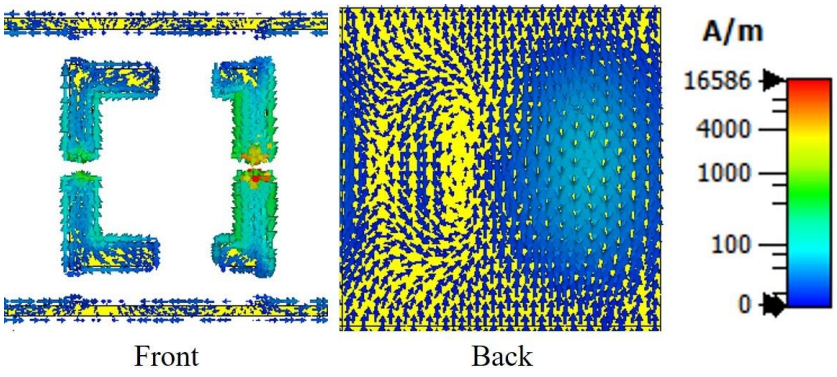

Figure 9. *Surface-current distribution on the MA at the second absorption frequency of 6.9 GHz corresponding to the applied voltage of 19V.*

4. CONCLUSIONS

In this study, we have presented the designs and conducted numerical investigations on electrically reconfigurable single- and dual-band MAs operating within the C band. By leveraging the adjustable varactor diode, the total effective capacitance in the equivalent LC model of the MAs can be actively tuned, thereby enabling the modulation of absorption frequencies through variations in the applied voltage. The resonance nature of the absorption phenomenon has been confirmed through comprehensive analysis. Additionally, we have demonstrated that introducing asymmetry to the resonator structure can effectively modify the interaction between the MA and the incident wave, resulting in an increased number of absorption resonance peaks. The controllability of the absorption characteristics through applied bias voltages highlights the potential of this MA design for a wide range of applications, including electromagnetic wave absorption, communication systems, and radar technologies. Furthermore, it is worth noting that further investigations and optimizations of the MA structure and material properties hold promise for achieving even higher efficiency in absorption behavior, thus expanding the potential applications in diverse domains that require effective control and manipulation of electromagnetic waves.

Acknowledgement: *This research is funded by Vietnam National Foundation for Science and Technology Development (NAFOSTED) under grant number 103.99-2020.23.*

REFERENCES

[1]. A. B. Devarapalli, T. Moyra, *"Design of a metamaterial loaded W-shaped patch antenna with FSS for improved bandwidth and gain"*, Silicon, 15, 2011-2024 (2023).

[2]. C. M. Saleh, E. Almajali, A. Jarndal, J. Yousaf, S. S. Alja'Afreh, R. E. Amaya, *"Wideband 5G antenna gain enhancement using a compact single-layer millimeter wave metamaterial lens"*, IEEE Access, 11, 14928-14942 (2023).

[3]. W. J. Padilla, R. D. Averitt, *"Imaging with metamaterials"*, Nature Reviews Physics, 4, 85-100 (2022).

[4]. Y. Roh, S.-H. Lee, J. Kwak, H. S. Song, S. Shin, Y. K. Kim, J. W. Wu, B.-K. Ju, B. Kang, M. Seo, *"Terahertz imaging with metamaterials for biological applications"*, Sensors and Actuators B: Chemical, 352(1), 130993 (2022).

[5]. H. Lee, D.-H. Kwon, *"Microwave metasurface cloaking for freestanding objects"*, Physical Review Applied 17, 054012 (2022).

[6]. N. Wu, Y. Jia, C. Qian, H. Chen, *"Pushing the limits of metasurface cloak using global inverse design"*, Advanced Optical Materials 11(7), 2202130 (2023).

[7]. W. Shahzad, W. Hu, Q. Ali, H. Raza, S. M. Abbas, L. P. Ligthart, *"A low-cost metamaterial sensor based on DS-CSRR for material characterization applications"*, Sensors 22(5), 2000 (2022).

[8]. S. Shen, X. Liu, Y. Shen, J. Qu, E. Pickwell-MacPherson, X. Wei, Y. Sun, *"Recent advances in the development of materials for terahertz metamaterial sensing"*, Advanced Optical Materials 10(1), 2101008 (2022).

[9]. N. I. Landy, S. Sajuyigbe, J. J. Mock, D. R. Smith, W. J. Padilla, *"Perfect metamaterial absorber"*, Physical Review Letters 100, 207402 (2008).

[10]. Z. Huang, B. Wang, *"Ultra-broadband metamaterial absorber for capturing solar energy from visible to near infrared"*, Surfaces and Interfaces 33, 102244 (2022).

[11]. P. D. Tan, D. T. Ha, B. S. Tung, B. X. Khuyen, D. T. Chi, V. D. Lam, L. Chen, H. Zheng, Y. P. Lee, *"Recoverable broadband absorption based on ultra-flexible meta-surfaces"*, Crystals 12, 1817 (2022).

[12]. M. Bennaoum, M. Berka, A. Bendaoudi, A. Y. Rouabhi, Z. Mahdjoub, *"Investigation of a near-perfect quad-band polarization-insensitive metamaterial absorber based on dual-T circular shaped resonator array designed on a silicon substrate for C-, X- and Ku-bands applications"*, Silicon 15, 699-712 (2023).

[13]. M. Zhong, *"Measurement and verification of a multi-band terahertz metamaterial absorber based on multiple coupling effects"*, Infrared Physics and Technology 128, 104506 (2023).

[14]. R. M. H. Bilal, S. Zakir, M. A. Naveed, M. Zubair, M. Q. Mehmood, Y. Massoud, *"Nanoengineered nickel-based ultrathin metamaterial absorber for the visible and short-infrared spectrum"*, Optical Materials Express 13(1), 28-40 (2023).

[15]. B. X. Khuyen, B. S. Tung, Y. J. Yoo, Y. J. Kim, K. W. Kim, L.-Y. Chen, V. D. Lam, Y. P. Lee, *"Miniaturization for ultrathin metamaterial perfect absorber in the VHF band"*, Scientific Reports 7, 45151 (2017).

[16]. G. Deng, Z. Yu, J. Yang, Z. Yin, Y. Li, B. Chi, *"A miniaturized 3-D metamaterial absorber with wide angle stability"*, IEEE Microwave and Wireless Components Letters 32(9), 1111-1114 (2022).

[17]. X. Sun, Z. Qu, J. Yuan, Q. Wang, *"Reconfigurable broadband polarisation conversion metasurface based on VO_2"*, Photonics and Nanostructures - Fundamentals and Applications 50, 101012 (2022).

[18]. H. Feng, Z. Zhang, J. Wang, J. Zhang, D. Fang, C. Liu, G. Wang, Y. Gao, Y. Gao, *"Individually frequency and amplitude tunable metamaterial absorber with sensing functions based on strontium titanate and graphene",* Diamond and Related Materials 130, 109455 (2022).

[19]. L. V. Long, N. H. Tung, T. T. Giang, P. T. Son, N. T. Tung, B. S. Tung, B. X. Khuyen, V. D. Lam, *"Rotary bi-layer ring-shaped metamaterials for reconfiguration absorbers",* Applied Optics 61(30), 9078-9084 (2022).

[20]. R. Yang, F. Zhang, Z. Li, Q. Fu, Y. Fan, *"Controllable electromagnetically induced transparency in an electrically tunable terahertz hybrid metasurface"*, Optics & Laser Technology 163, 109380 (2023).

[21]. X. Zhao, K. Fan, J. Zhang, H. R. Seren, G. D. Metcalfe, M. Wraback, R. D. Averitt, X. Zhang, *"Optically tunable metamaterial perfect absorber on highly flexible substrate"*, Sensors and Actuators A: Physical 31, 74-80 (2015).

[22]. H. L. Wang, Y. K. Zhang, T. Y. Zhang, H. F. Ma, T. J. Cui, *"Broadband and programmable amplitude-phase-joint-coding information metasurface"*, ACS Applied Materials & Interfaces 14(25), 29431–29440 (2022).

[23]. L. Shao, W. Zhu, *"Electrically reconfigurable microwave metasurfaces with active lumped elements: a mini review"*, Frontiers in Materials 8, 689665 (2021).

[24]. F. Yang, P. Pitchappa, N. Wang, *"Terahertz Reconfigurable Intelligent Surfaces (RISs) for 6G Communication Links"*, Micromachines 13(2), 285 (2022).

[25]. CST Microwave Studio. Dassault Systèmes. http://www.cst.com.

[26]. J. Zhao, Q. Cheng, J. Chen, M. Q. Qi, W. X. Jiang, T. J. Cui, *"A tunable metamaterial absorber using varactor diodes"*, New Journal of Physics 15, 043049 (2013).

[27]. J. Zhou, E. N. Economou, T. Koschny, C. M. Soukoulis, *"Unifying approach to lef-handed material design"*, Optics Letters 31, 3620-3622 (2006).

[28]. B. X. Khuyen, B. S. Tung, Y. J. Kim, J. S. Hwang, K. W. Kim, J. Y. Rhee, V. D. Lam, Y. H. Kim, Y. P. Lee, *"Ultra-subwavelength thickness for dual/triple-band metamaterial absorber at very low frequency"*, Scientific Reports 8, 11632 (2018).

TÓM TẮT

Vật liệu biến hóa hấp thụ sóng điện từ trong vùng C được điều khiển bằng điện áp ngoài

Vật liệu biến hóa hấp thụ sóng điện từ có thể điều khiển đặc tính đã thu hút được sự chú ý đáng kể nhờ vào khả năng chủ động điều khiển các tính chất hấp thụ mà không làm thay đổi cấu trúc hình học nội tại. Nghiên cứu này đề xuất một cách tiếp cận đơn giản để tạo ra các vật liệu biến hóa hấp thụ sóng điện từ có thể điều khiển được bằng điện áp ngoài thông qua việc tích hợp các điốt biến dung. Nội dung nghiên cứu được trình bày bao gồm hai loại vật liệu khác nhau: vật liêu biến hóa hấp thụ đơn tần và vật liệu biến hóa hấp thụ băng tần kép. Bằng cách sử dụng điện áp ngoài, tính chất hấp thụ của vật liệu có thể kiểm soát hiệu quả trong vùng tần số thuộc dải C. Nguyên lý hoạt động cơ bản của vật liệu biến hóa đã được làm rõ, ở đó, việc kiểm soát sự biến đổi giá trị các tham số hiệu dụng của điốt tích hợp đã giúp điều chỉnh tần số cộng hưởng từ của vật liệu biến hóa đề xuất. Kết quả nghiên cứu của chúng tôi có thể góp phần trong việc gia tăng hiệu suất, khả năng điều khiển linh hoạt và khả năng thích ứng của các thiết bị dựa trên vật liêu biến hóa được trang bị các chức năng nâng cao cho các ứng dụng đa dạng trong lĩnh vực viễn thông, che chắn điện từ và nhiều ứng dụng khác.

Từ khoá: Vật liêu biến hóa hấp thụ sóng điện từ được điều khiển bằng điện áp ngoài; Điốt biến dung; Cộng hưởng từ.